

Refill Friction Stir Spot Welding of 2198-T8 Aluminum Alloy

Yao Shi¹ · Yumei Yue¹ · Liguozhang¹ · Shude Ji¹ · Yue Wang¹

Received: 13 March 2017 / Accepted: 4 May 2017 / Published online: 27 May 2017
© The Indian Institute of Metals - IIM 2017

Abstract Refill friction stir spot welding (RFSSW) technology was used to weld 2 mm-thick 2198-T8 aluminum alloy in this work. As one of the most significant factors affecting the joint mechanical properties, effect of the tool rotating speeds on microstructure and mechanical properties of the RFSSW joint was mainly discussed. Results showed that keyhole could be successfully refilled after the RFSSW process. Due to the complicated movement of the tool components, different material flow behaviors could be obtained at the pin affected zone and sleeve affected zone, leading to different microstructures at the two regions. By undergoing through different heat cycle during welding, the secondary phase particles (Al_2Cu) showed different morphologies and sizes at different regions. The lap shear failure load of the joint firstly increased and then decreased with increasing in the rotating speed. The maximum failure load of 9298 N was obtained when using 1600 rpm. All the joints showed lap-shear fracture mode.

Keywords Refilling friction stir spot welding · 2198-T8 aluminum alloy · Microstructure · Secondary phase particles · Lap shear failure load

1 Introduction

Being a solid state joining technology, friction stir spot welding (FSSW) has been invented by Mazda Corporation in 2003 [1]. Similar to friction stir welding (FSW), welding temperatures during the FSSW process does not exceed the melting points of the base material (BM) [2]. Hence, plenty of fusion defects such as pores and hot cracks can be avoided during FSSW [3]. Besides, FSSW joint owns other advantages such as smaller distortion, lower residual stress and longer fatigue lives [4].

FSSW has originally been invented to join aluminum alloys. Compared with other spot joining technologies such as riveting and resistance spot welding, FSSW process needs no pre-holing before welding and no weight increase is observed after welding [5]. The FSSW process is also easily handled and environmental friendly. According to Mazda Corporation, a FSSW joint requires 99% less energy than a RSW joint. So far, the FSSW joint has been widely used in many industrial structures, such as the rear door of Mazda RX-8 car and some structures of Toyota cars [6–9].

Due to the characteristic of the FSSW process, one typical feature after the welding process is that a keyhole which owns the same size of the rotating pin remains at the joint center [10]. The keyhole destroys the joint continuity and can induce serious stress concentration when FSSW joint bears external force. Furthermore, body paint can hardly reach the keyhole bottom, deteriorating the joint anti-corrosion properties [8, 11–13]. Therefore, lots of works have been done by researchers to repair the keyhole [14–19].

Han et al. [15] used a 7075 aluminum alloy bit to refill the keyhole which was left in 2219 aluminum alloy FSW joint and attained joint with satisfied mechanical

✉ Yumei Yue
yueyumei999@yeah.net

✉ Shude Ji
superjsd@163.com

¹ Faculty of Aerospace Engineering, Shenyang Aerospace University, Shenyang 110136, People's Republic of China

properties. Ji et al. [16] used an active–passive filling method to fill the keyhole in AZ31B magnesium alloy and attained joint related tensile strength equivalent to 96.3% of the defect-free FSW joint. Zhang et al. [18] filled the keyhole using a pinless tool and a T shaped filler bit and found out that the T shaped filler was better than the cylindrical filler. By adopting a series of non-consumable tools with gradual changed geometries, Zhou et al. [19] filled the keyhole of the 316L stainless steel and attained joint with higher tensile strength than the base material (BM).

Refill friction stir spot welding (RFSSW) is a new method, which has been invented by GKSS in 2002 [20]. The tool system used in RFSSW consists of three components: a clamping, a sleeve and a pin [21]. By exerting a relatively complicated movement to the three components, the plastic material which is squeezed out by the tool can be refilled back into the joint after welding. Hence spot joint without keyhole can be obtained [22]. Since invention, RFSSW process has been used to weld some kind of materials and some important conclusions have been concluded [10–13, 23–25]. Shen et al. [24] studied the microstructure and mechanical properties of 7075-T6 aluminum alloy RFSSW joint and found out that the main feature affecting the joint mechanical properties was the bonding ligament and the connecting qualities of the stir zone/thermo-mechanically affected zone (SZ/TMAZ) interface. Similar conclusion was also obtained by Li et al. [10]. Reimann et al. [25] refilled the keyhole with 7.5 mm diameter in 6061-T6 aluminum alloy sheets and found out that the joint failed at the heat affected zone (HAZ). Tier et al. [11] studied the microstructure and mechanical properties of 5042-O RFSSW joint and found out that lower rotating speed resulted in higher lap shear failure load. Li et al. [10] found out that the impact strength of the 2024 RFSSW joint was better than the BM. Besides, Gonçalves et al. [26] used RFSSW to join carbon fiber-reinforced polyamide 66 laminate and obtained joints with excellent mechanical properties.

Because of high strength and excellent corrosion resistance of 2000s aluminum alloys, they are widely used in aerospace industries. 2198-T8 is a typical (Al–Cu–Li) alloy with low density, high tensile strength, high toughness and corrosion performance. Pieta et al. [23] used RFSSW to weld 3.2 mm-thick 2198-T8 aluminum alloy sheet and investigated the effect of welding parameters on joint lap shear failure load. However, the effect of welding parameters on the microstructure and the relation between the microstructure and mechanical properties are yet to be addressed. Therefore, in this work, RFSSW has been used to weld 2 mm-thick 2198-T8 aluminum alloy. The focus of the present study is on the effect of tool rotating speed on the microstructure and lap shear failure load of the RFSSW joint.

2 Experimental Procedures

In this work, 2 mm-thick 2198-T8 was chosen as the BM. All the sheets were cut to the dimensions of 140 mm × 40 mm. Before welding, surfaces of all the sheets were polished with emery papers to wipe off the oxide layer. Two sheets were lap combined and welded in the center of the overlap area. The lap shear specimen is shown in Fig. 1. The RFSSW machine used during the experimental investigation was RPS100 SK10. Outer diameters of the pin, the sleeve and the clamping ring were 5.2, 9 and 14.5 mm, respectively. During welding, tool rotational speeds of 1200, 1400, 1600 and 1800 rpm were used. Other welding parameters such as sleeve plunge depth, dwell time, plunge speed and refilling speed were 2.6 mm, 0.5 s, 60 mm/min and 60 mm/min, respectively.

After welding, metallographic samples were cut using an electrical discharge cutting machine. Metallographic samples were etched with Keller's reagent (95 ml H₂O, 2.5 ml HNO₃, 1.5 ml HCL and 1 ml HF) for 20 s. The metallographic analyses were carried out by optical microscopy (OM VHX-1000E) and a scanning electron microscope (SEM FEI Quanta 200F). Lap shear tests were carried out using a computer-controlled universal tensile testing machine using a constant speed of 5 mm/min at room temperature. All the experimental results were attained by averaging the results of no less than three samples. After that, fracture surfaces were observed using the VHX-1000E and fracture morphologies were observed using SEM (SU3500).

3 Results and Discussion

Figure 2 shows the cross sections of the RFSSW joint using different rotating speeds. It can be seen in Fig. 2a that the keyhole can be successfully refilled after RFSSW. On the whole, the morphology of the SZ shows a basin-like morphology. At the joint center, a region, which

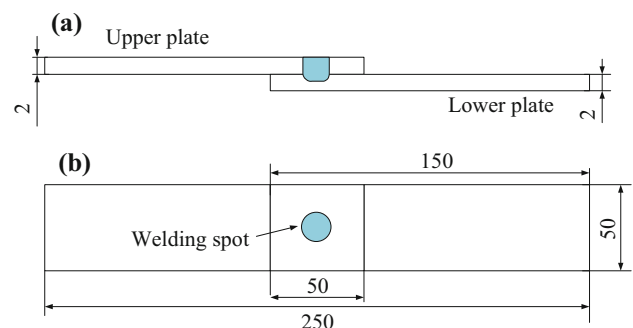


Fig. 1 Dimensions of the lap shear specimen: **a** side view and **b** top view

shows relatively light colour can be observed. This region is formed due to the weak material flow behavior during the welding process, which will be discussed in the

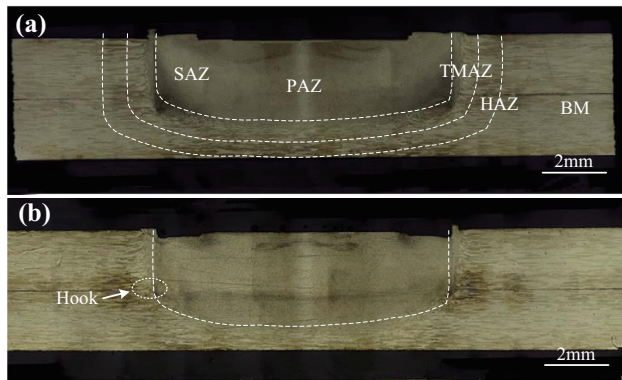


Fig. 2 Cross sections of the RFSSW joints using different rotating speeds: **a** 1200 rpm and **b** 1600 rpm

following section. As shown in Fig. 2b, with the increase in the rotating speed, the joint cross section shows little difference compared to the joint shown in Fig. 2a. As shown in Fig. 3a, void defects can be observed at the maximum plunge depth region while using 1200 rpm, which can be attributed to weak material flow behavior when using low rotating speed. The void can be eliminated by increasing the rotating speed, as shown in Fig. 3b. Void defect is a serious volume defect. It can induce serious stress concentration and lead to bad corrosion resistance. Figure 3c, d show the TMAZ/SZ interface using different rotating speeds. It can be seen that when using 1200 rpm, the interface is rather obvious. The grains show rather different morphologies at the two sides of the interface, indicating relatively weak bonding. When using high rotating speed (1600 rpm), well bonding condition can be observed at the interface, as shown in Fig. 3d. Different bonding conditions of the TMAZ/SZ

Fig. 3 Defects of the RFSSW joints: voids using **a** 1200 rpm and **b** 1600 rpm, TMAZ/SZ interface using **c** 1200 rpm and **d** 1600 rpm, **e** hook using 1200 rpm

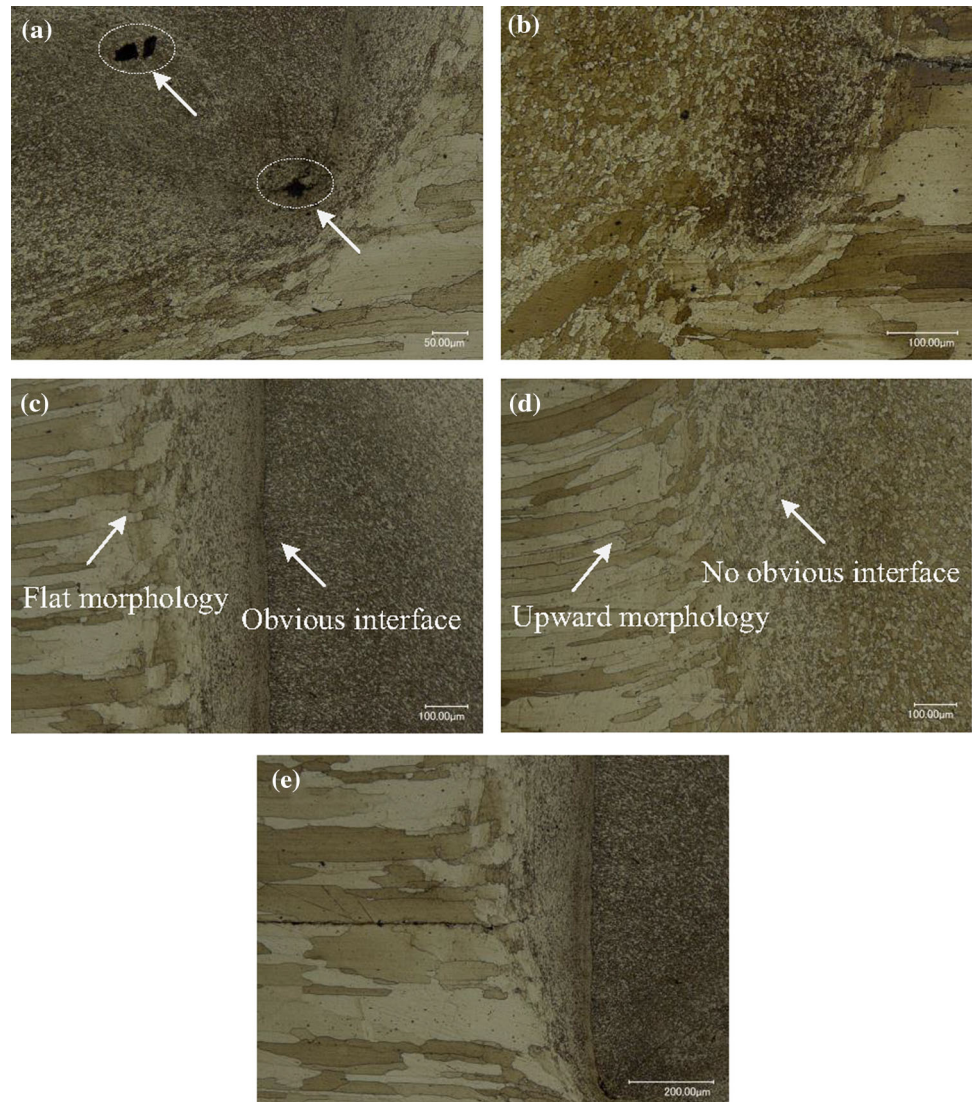
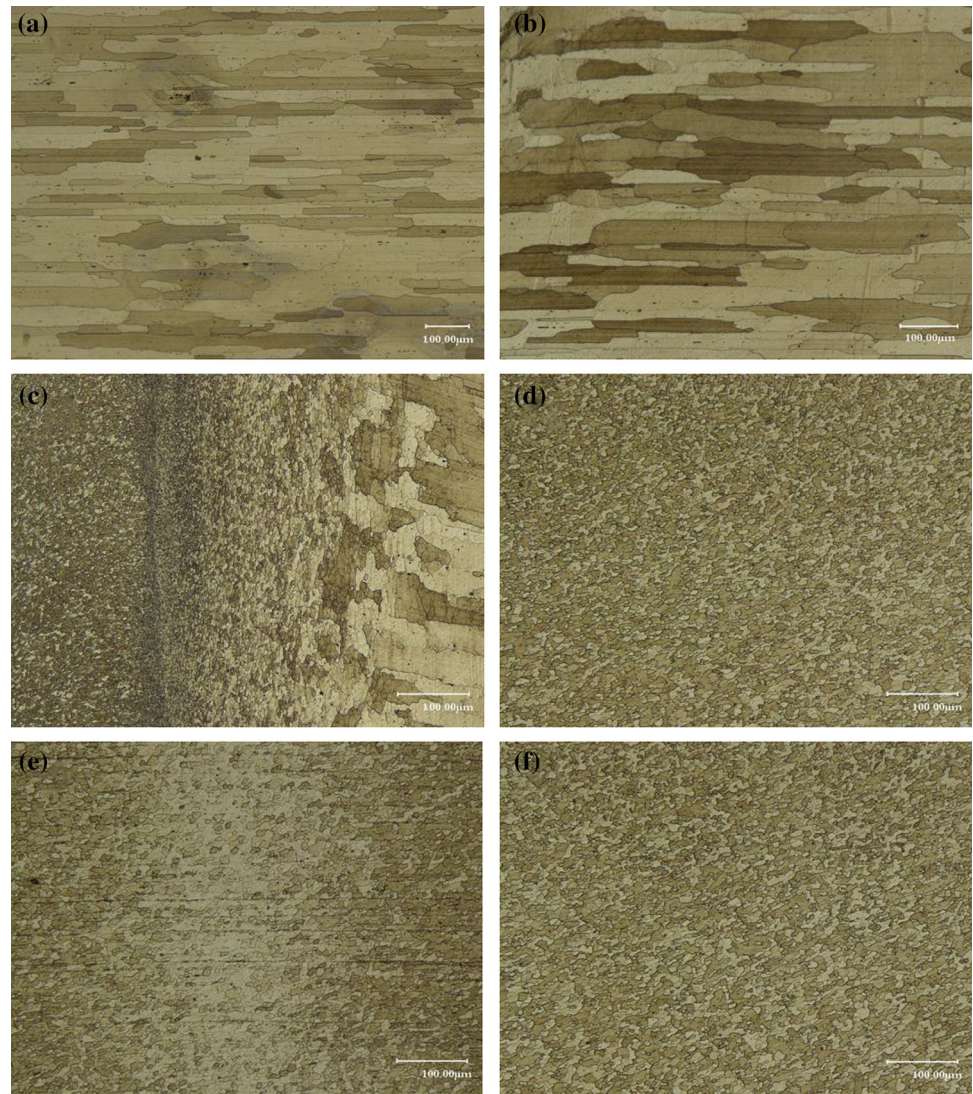


Fig. 4 Microstructure of the RFSSW joint: **a** BM, **b** HAZ, **c** TMAZ, **d** SAZ using 1200 rpm, **e** PAZ and **f** SAZ using 1600 rpm



interface may lead to different fracture modes of the joint. As introduced by Shen et al. [24], the TMAZ/SZ interface is the weak region of the RFSSW joint, which can be also observed in the present work. Adjacent to the SZ, the original lap interface shows a slight upward bending morphology, which is called hook. During the lap shear test, hook is always the crack initiation region. It can be seen in Fig. 3e that the hook shows a rather flat morphology. For lap joint, hook height is an important factor affecting the joint mechanical properties. It can reduce the effective sheet thickness and therefore detrimental to joint lap shear properties.

Similar to the conventional FSW joint, microstructure of the RFSSW joint can be divided into BM, TMAZ, HAZ and SZ, as indicated in Fig. 2a. Figure 4 shows the microstructures at different regions of the joint. As shown in Fig. 4a, grains of the 2198-T8 aluminum alloy show long morphologies with irregular boundaries. Some very

small black spots can be seen in the grains and at the grain boundaries. These black spots are the secondary phase particles. These secondary phase particles will be discussed in the following part. Going through the heat cycle during welding makes the grains at the HAZ obviously much coarser compared to the BM, as shown in Fig. 4b. The small secondary phase particles can still be observed in smaller quantities. The TMAZ undergoes both moderate mechanical stirring and heat cycle during welding. Therefore the grains of the TMAZ show rather non-uniform morphologies, as shown in Fig. 4c. As shown in Fig. 4d, in the SZ, complete dynamic recrystallization (DRX) happens and fine equiaxed grains are observed. It should be noted that for the RFSSW joint, the microstructure of the SZ can also be divided into the pin affected zone (PAZ) and the sleeve affected zone (SAZ), as denoted in Fig. 2a. The SAZ is the region where the material is mainly stirred by the sleeve and therefore shows fine sizes. The PAZ is the

Fig. 5 Distribution of the secondary particles of the RFSSW joint (1200 rpm): **a** BM, **b** HAZ, **c** TMAZ and **d** SZ

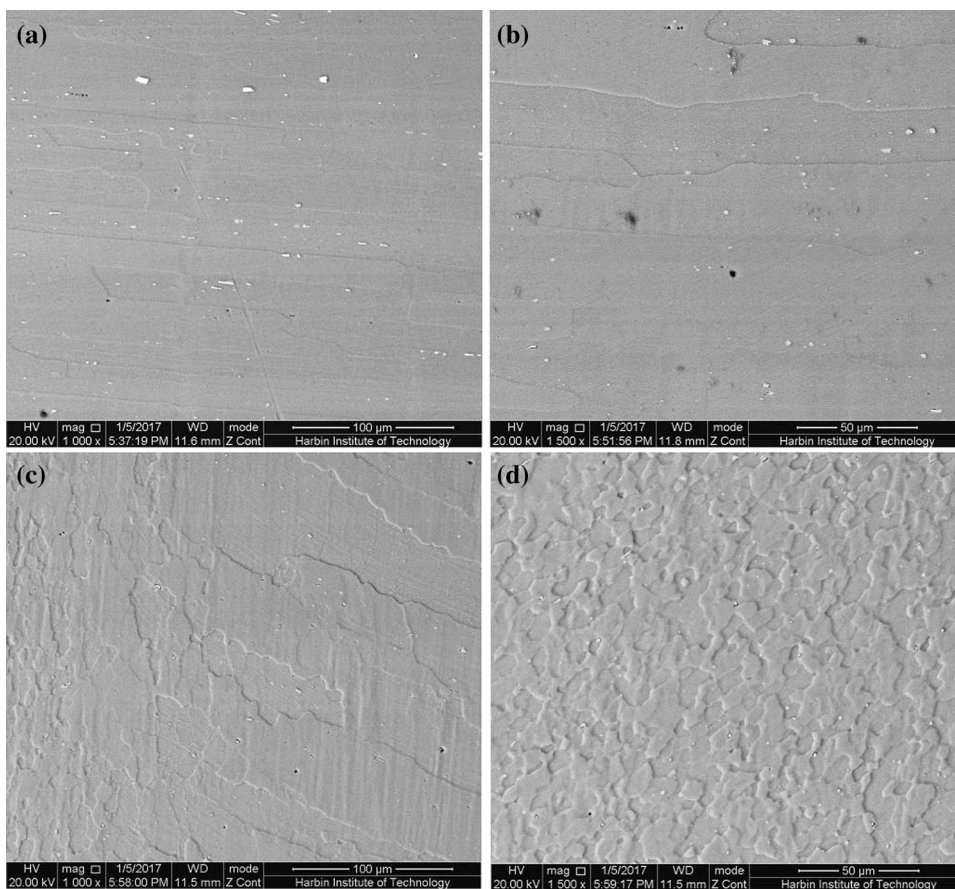
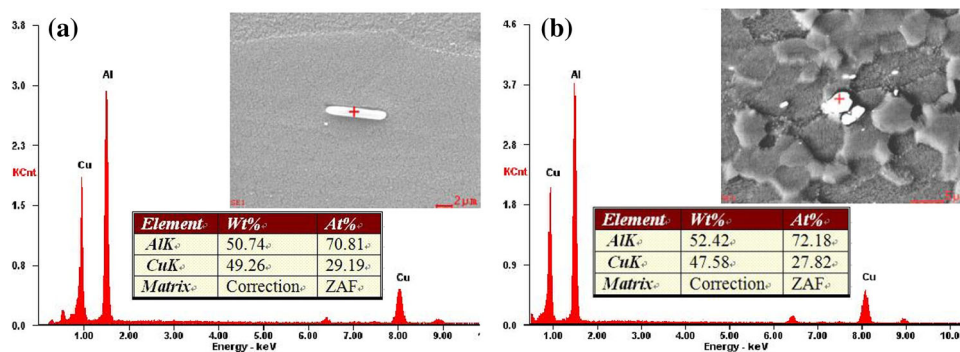


Fig. 6 EDS analysis of the secondary particle at (a) the BM and (b) the SZ



region at the joint center, where the material is not directly stirred by the pin or sleeve and therefore the grains show a little coarser morphologies compared with the SAZ, as shown in Fig. 4e. As shown in Fig. 4f, with the increase in the rotational speed, more frictional heat is produced, leading to grains coarseness.

Figure 5 shows the secondary phase particles at different regions of the RFSSW joint. Compared to the OM morphologies, the secondary particle phases show different morphology when using SEM, which are recognized as the white spots. As shown in Fig. 5a, lots of the secondary phase particles with different sizes can be observed in the

BM. They can be observed both in the grains and at the grain boundaries. As shown in Fig. 5b, less secondary phase particles can be observed at the HAZ, which can be attributed to the dissolution caused by the heat cycle during welding. Similar to the HAZ, much less secondary phase particles can be observed at the TMAZ region. That is because the TMAZ reaches higher temperature and undergoes more violent material flow behavior during welding. Figure 5d shows the secondary phase particles at the SZ region. It can be seen that almost no secondary phase particles can be observed at the SZ. And the morphology is rather different from that at the BM region.

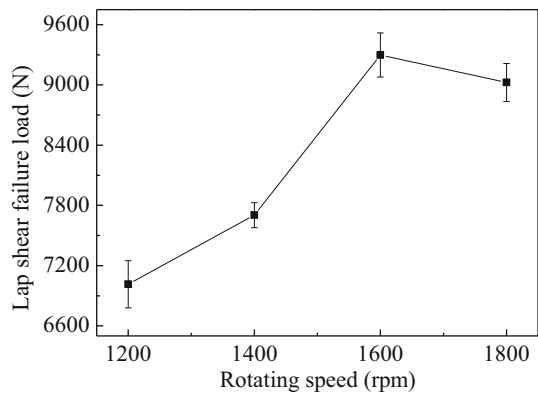


Fig. 7 Lap shear failure load of the joints

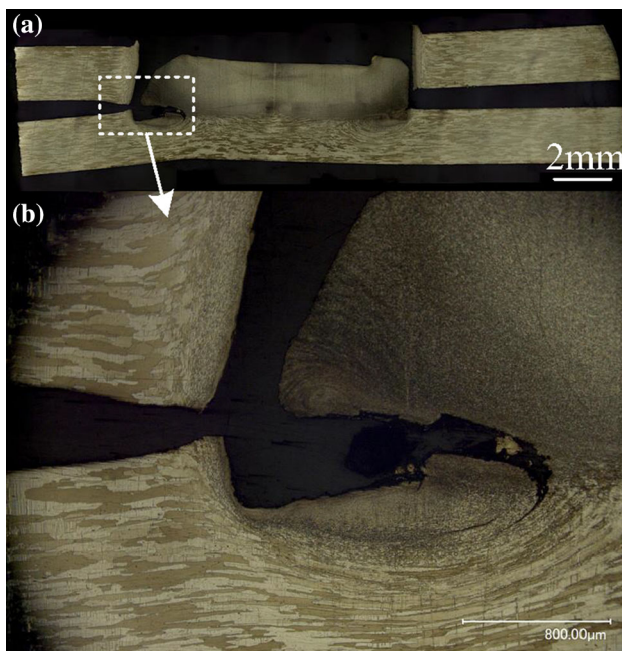


Fig. 8 Shear-plug fracture mode of the RFSSW joint: **a** cross section and **b** magnified view of the fracture path

Figure 6 shows the EDS analysis of the secondary phase particles at the BM and the SZ. It is worth mentioning is that, the SEM and EDS analysis have been done after etching in order to get a clearer image. As shown in Fig. 6a, the long cylindrical secondary phase particles are the Al–Cu phase. The element ratio is very close to the Al_2Cu phase. As shown in Fig. 6b, the secondary phase at the SZ mainly shows circular morphology. The element ratio is also very close to the Al_2Cu phase. Similar to the FSW process, the RFSSW process is a rather complicated process. It includes grain breaking, dynamic recrystallization, precipitation and dissolution of the secondary phase particles. It can be seen in Fig. 5 that the grain morphologies in the SZ are mainly influenced by the dynamic recrystallization. The secondary phase particles in Fig. 6

are mainly influenced by precipitation and dissolution process.

Figure 7 shows the lap shear failure load of the RFSSW joints using different rotating speeds. It can be seen that with the increase in the rotating speed, lap shear failure load of the joint increases at the beginning and then decreases. The maximum failure load of 9298 N is attained with 1600 rpm rotating speed. During the lap shear test, all joints present the shear-plug fracture mode, as shown in Fig. 8. It can be seen that the main fracture positions are the TMAZ/SZ interface. The SZ remains at the lower sheet after the lap shear test. Besides, it can be seen in Fig. 8 that at the left side of the weld nugget, a crack, which propagates through the void, can also be recognized, as shown in Fig. 8b. Hence, when the rotating speed increases from 1200 to 1600 rpm, the increase in the lap shear failure load can be attributed to the void elimination. With further increase in the rotating speed, the decrease of the lap shear failure load can be attributed to the grains coarseness (Fig. 4).

Figure 9 shows the fracture morphologies of the shear-plug fracture mode. Figure 9a is the general view of the TMAZ/SZ interface. It can be seen that there exist different morphologies at different regions. Figure 9b shows the top region of the TMAZ/SZ interface. Some ridge-like structures, which are formed due to the weak bonding of the TMAZ/SZ interface can be seen. Similar to Fig. 9b, no dimples can be observed in Fig. 9c. Figure 9d, e show the fracture morphologies of the lower regions of the TMAZ/SZ interface. The rotating trace of the weld nugget can be clearly recognized.

4 Conclusions

2 mm-thick 2198-T8 aluminum alloy has been welded in the present work using RFSSW technology. The effect of the tool rotating speeds on the microstructure and mechanical properties of the RFSSW joint has mainly been discussed. The following conclusions can be drawn.

- (1) Keyhole can be successfully refilled using RFSSW. A small void can be observed at the maximum plunge depth region and the void can be eliminated with increasing the rotating speed.
- (2) The SAZ and the PAZ show different microstructure morphologies due to different material flow behaviors. The secondary phase particles (Al_2Cu) show different morphologies and sizes at different regions.
- (3) With the increase in the rotating speed from 1200 to 1800 rpm, lap shear failure load of the joint increases at the beginning and then decreases with the increase in the rotating speed. The maximum failure load of 9298 N is attained when using 1600 rpm.

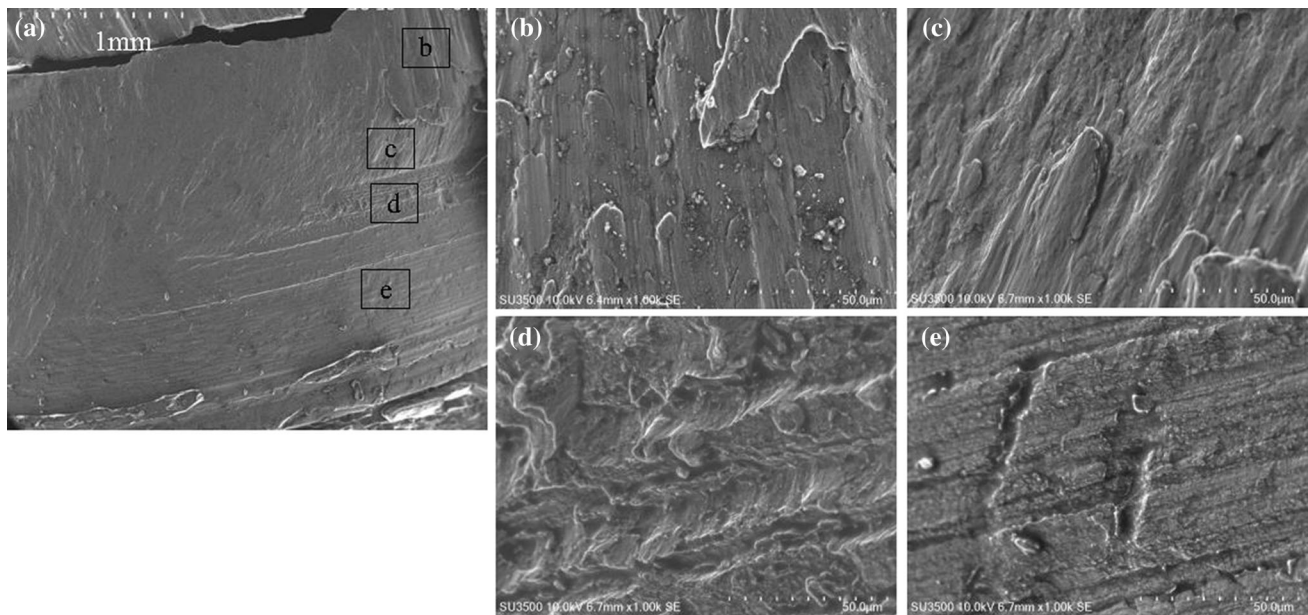


Fig. 9 Fracture morphologies of the shear-plug fracture mode: **a** general view of the TMAZ/SZ interface, **b** region *b*, **c** region *c*, **d** region *d* and **e** region *e* marked in *a*

- (4) During the lap shear test, all the joint show lap-shear fracture mode due to the weak bonding at the TMAZ/SZ interface.

Acknowledgements This work is supported by the National Natural Science Foundation of China (Nos. 51204111 and 51405309).

References

- Ji S, Wang Y, Li Z, Yue Y, and Chai P, *Trans Indian Inst Met* (2016) DOI [10.1007/s12666-016-0937-1](https://doi.org/10.1007/s12666-016-0937-1).
- Li W Y, Li J F, Zhang Z H, Gao D L, Wang W B, and Dong C L, *Mater Des* **62** (2014) 247.
- Badarinarayan H, Yang Q, and Zhu S, *Int J Mach Tool Manuf* **49** (2009) 148.
- Xu R Z, Ni D R, Yang Q, Liu C Z, and Ma Z Y, *J Mater Sci Technol* **32** (2016) 326.
- Lathabai S, Painter M, Cantin G, and Tyagi V, *Scripta Mater* **55** (2006) 899.
- Zhang Z H, Li W Y, Feng Y, Li J L, and Chao Y J, *Mater Sci Eng A* **598** (2014) 312.
- Venukumar S, Muthukumar S, Yalagi S, and Kailas S, *Int J Fatigue* **61** (2014) 93.
- Uematsu Y, Tokaji K, Tozaki Y, Kurita T, and Murata S, *Int J Fatigue* **30** (2008) 1956.
- Pan T, Santella M, and Blundell N, *SAE Int J Mater Manuf* **2**(1) (2009) 23.
- Li Z, Gao S, Ji S, Yue Y, and Chai P, *J Mater Eng Perform* **25** (2016) 1673.
- Tier M, Rosendo T, dos Santos J, Huber N, Mazzaferro J, Mazzaferro C, and Strohaecker T, *J Mater Process Tech* **213** (2013) 997.
- Shen Z, Yang X, Yang S, Zhang Z, and Yin Y, *Mater Des* **54** (2014) 766.
- Suhuddin U, Fischer V, and dos Santos J, *Scripta Mater* **68** (2013) 87.
- Huang Y, Han B, Tian Y, Liu H, Lv S, Feng J, Leng J, and Li Y, *Sci Technol Weld Join* **16** (2011) 497.
- Han B, Huang Y, Lv S, Wan L, Feng J, and Fu G, *Mater Des* **51** (2013) 25.
- Ji S, Meng X, Zeng Y, Ma L, and Gao S, *Mater Des* **97** (2016) 175.
- Ji S, Meng X, Huang R, Ma L, and Gao S, *Mater Sci Eng A* **664** (2016) 94.
- Zhang G, Jiao W, and Zhang J, *Sci Technol Weld Join* **19** (2014) 98.
- Zhou L, Liu D, Nakata K, Tsumura T, Fujii H, Ikeuchi K, Michishita Y, Fujiya Y, and Morimoto M, *Sci Technol Weld Join* **17** (2012) 649.
- Gao C, Gao R, and Ma Y, *Mater Des* **83** (2015) 719.
- Zhao Y, Liu H, Lin Z, Chen S, and Hou J, *Sci Technol Weld Join* **19** (2014) 617.
- Gao C, Ma Y, Tang L, Wang P, and Zhang X, *Mater Des* **115** (2017) 224.
- Pieta G, dos Santos J, Strohaecker T, and Clark T, *Mater Manuf Process* **29** (2014) 934.
- Shen Z, Yang X, Zhang Z, Cui L, and Li T, *Mater Des* **44** (2012) 476.
- Reimann M, Gartner T, Suhuddin U, Göbel J, and dos Santos J, *J Mater Process Tech* **237** (2016) 12.
- Gonçalves J, dos Santos J, Canto L, and Amancio-Filho, S, *Mater Lett* **159** (2015) 506.